Design and Modeling of an 80 bar Oxy-Combustor for Direct Fired Supercritical CO_2 Applications

Peter A. Strakey and Todd G. Sidwell
National Energy Technology Laboratory
Morgantown, WV 26507
peter.strakey@netl.doe.gov

ABSTRACT

As supercritical CO_2 power cycles for fossil energy power generation continue to generate interest, there are significant issues and unanswered questions regarding injector design, flame stabilization, wall heat transfer, CO emissions, combustion dynamics and other combustion phenomenon. For natural gas, direct-fired cycles with carbon capture it is believed that Computational Fluid Dynamics (CFD) modeling will play an essential role in the combustor design process. To accurately model turbulent reacting flows at these unique conditions, experimental data is needed to validate CFD codes and sub-models and is currently lacking at conditions relevant for these cycles.

This paper presents the conceptual design and CFD simulations of an experimental 80 bar oxy-combustion facility and test article currently under construction at NETL. The facility is targeted towards the testing of a single injector, direct-fired sCO_2 combustor at the 100 kW thermal output level. While these conditions do not reflect the actual Allam cycle operating conditions (300 bar) they are viewed as a stepping stone in the model validation process at supercritical conditions.

Reynolds Averaged Navier-Stokes as well as Large Eddy Simulation are used to model the turbulent combustion process and aid in the design of the combustor and injector. Process parameters including oxidizer preheat temperature and combustor flowrate are investigated.

INTRODUCTION

As direct-fired sCO_2 power cycles are closer than ever to being demonstrated [1], there is still a profound lack of experimental data for designing combustors and validating CFD models [2,3]. Most of the combined experience within the combustion community in designing and modeling combustors is at pressures below 30 bar. Very little data exists for combustors operating at pressures relevant to the Allam cycle (300 bar) which is the current target for direct fired sCO_2 power cycles.

A numerical study of a gas turbine combustor operating in excess of 60 bar was conducted by Evdokimov [4] which showed improvements to combustion efficiency and reductions in NOx and CO emissions through the use of mesoscale coaxial swirling jets. While this study was on an air-fired combustor, it did focus on combustor pressures higher than typical gas turbine combustors. Levy and Arfi [5] studied the effects of turbulence-chemistry interaction using a partially-stirred reactor model on NOx formation and showed the benefits of using computational fluid dynamics (CFD) on combustor design and optimization.

The Allam cycle [6-7] is a recuperated sCO_2 cycle with a modest temperature rise in the combustor. The typical conditions as outlined by the Allam cycle include a combustor operating pressure of 300 bar, an inlet temperature of 750 °C and an exit temperature of 1150 °C. The fuel can be either natural gas or coal syngas. The latest public data on the thermodynamic efficiency of the cycle are in excess of 58% (for the natural gas version) based on the Lower Heating Value (LHV) of the fuel. In order to maintain a combustor exit temperature of 1150 °C roughly 95% of the CO_2 must be recycled to the combustor with the balance being sequestered.

With the current Department of Energy (DOE) focus on carbon free power generation, the most attractive feature of the cycle is the ability to capture the CO_2 since the working fluid is nearly pure CO_2 at 300 bar after water condensation and removal. Since typical commercial CO_2 pipelines operate in the 80 to 210 bar range [8], no extra compression power is needed which is a major drawback of post-combustion CO_2 capture cycles.

For the natural gas fired version of this cycle, a stoichiometric amount of O_2 would be roughly 7% of the CO_2 flow by volume. The oxygen used in the cycle is produced by an Air Separation Unit (ASU) and thus the O_2 and CO_2 being injected into the combustor can be mixed in any ratio desired with the remainder of the CO_2 being added further downstream. An upper limit for O_2 concentration can be assumed to be about 30% by volume based on oxygen safety concerns in the recuperators. The lower limit of O_2 concentration would be about 7% by volume assuming all the recycled CO_2 is mixed in with the oxygen. These unique conditions including the high pressures, high recuperation temperatures and high CO_2 dilution levels make these combustion conditions significantly different from conventional air breathing gas turbines.

Since running experimental combustors at 300 bar is both expensive and challenging, there is virtually no experimental data publically available to validate CFD codes and sub models. Current efforts at the South West Research Institute are focused on the development of a 1MW high-pressure oxy-combustor with CO_2 dilution and oxidizer preheat [9]. This effort is also utilizing CFD as a key aspect of the design process.

During the past year, NETL has been in the process of designing a high-pressure oxy-combustion experiment at the Morgantown, WV campus. The combustor is designed to operate at 80 bar (as a compromise between safety, expense and relevance) at the 100 kW power level with oxidizer preheat temperatures up to 950 K. Since the critical point of CO_2 is 74 bar and 304 K, this combustor will be able to operate within the supercritical regime of CO_2. More importantly, these conditions represent a significant departure from conventional Brayton cycle operating conditions and are a stepping stone to validating CFD codes and sub models at conditions more relevant to the Allam cycle.

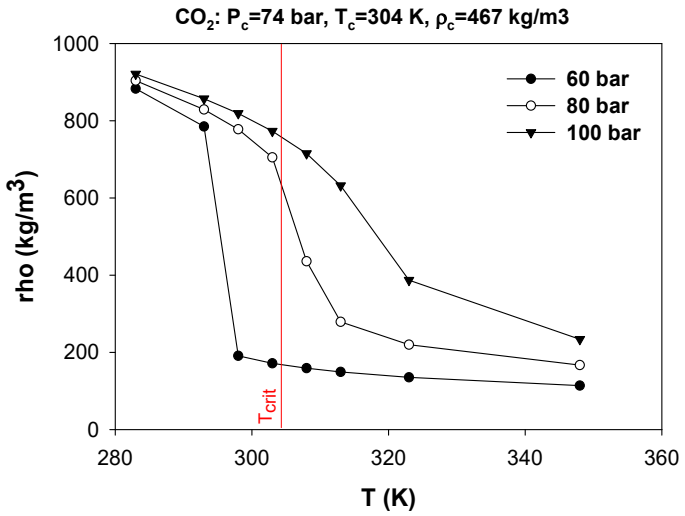

A plot of density verses temperature for pure CO_2 at several different pressures spanning a range around the maximum operating pressure of the combustor is shown in Figure 1. These data were calculated with the NIST Chemistry WebBook application [10] and demonstrate the very strong dependence of density on temperature near the critical temperature which is denoted by the vertical red line. While pure CO_2 would not be encountered in the injector due to mixing of O_2, pure CO_2 would be present near the combustor walls where it is being used as a coolant.

Figure 1: Density of CO_2 vs. temperature at three different pressures. From NIST Chemistry WebBook [7]. Vertical red line denotes critical temperature.

EXPERIMENTAL FACILITY

The combustor will be installed in the NETL Advanced Combustion Concepts Evaluation Laboratory (ACCEL), a former internal combustion engine laboratory which is currently being renovated to accommodate the combustor and associated hardware. To accommodate the high operating pressures, and a potential future increase in CO_2 and O_2 preheater thermal capacity, complete replacement of the facility process hardware was required. Detailed design of the process hardware and infrastructure have been completed and a process schematic is shown in Figure 2. The detailed design of the combustor, currently in progress, is discussed in detail in the following sections.

CH_4 and O_2 are supplied from arrays of standard 1A gas cylinders, while CO_2 is supplied as a liquid from an array of cryogenic dewars. These supplies are scalable and have been sized initially to provide sufficient capacity to run a minimum of 90 combustion tests of 30 second duration before refilling the supplies to their respective maximum capacities. The liquid CO_2 from the dewars is pumped to 137.9 bar and split into two streams: the primary stream, as combustion diluent; and the secondary stream, for liner effusion cooling. The primary CO_2 stream is heated to change the CO_2 phase to supercritical, while the O_2 stream is heated separately before mixing with the supercritical CO_2 stream. The temperature of the combined CO_2 and O_2 stream is maintained above 330 K to prevent excessive variation in CO_2 density and thermophysical properties during operation as shown in Figure 1. Water spray nozzles in the exhaust duct downstream of the combustor cool the combustor exhaust and disrupt shockwaves produced by expansion of the combustor exhaust stream to atmospheric pressure. Current supply sizes, pressures and temperatures, and nominal operating conditions are summarized in Table 1.

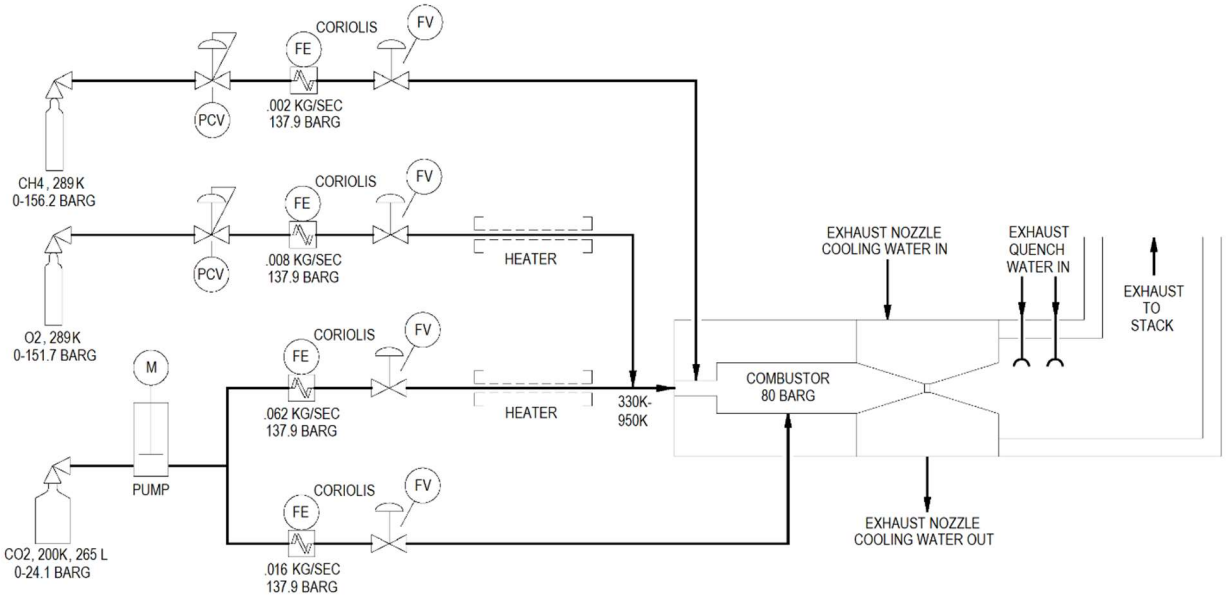

Figure 2: Flow Schematic of the NETL Supercritical CO_2 Oxy-Combustor Test Facility

Table 1: Process fluid conditions for supply system and combustor feed.

Process Fluid	Fluid Supply			Combustor Feed		
	Cylinder/ Dewar Size	Temp [K]	Max Pressure [bar]	Mass Flow [kg/s]	Temp [K]	Max Pressure [bar]
CH4	1A x 3	289	156	0.0020	289	138
O2	1A x 6	289	152	0.0080	330	138
CO2	265 l x 3	220	24	0.0620	330	138
Liner Cooling CO2				0.0155	289	138
Exhaust Cooling Water	Utility	289	4	0.3150	289	4

The basic process control system (BPCS) is based on an Allen-Bradley ControlLogix PLC with a workstation-based FactoryTalk HMI. Mass flow rates are measured by Micro Motion CMF Coriolis flow meters to within ±0.35% of reading. Process pressures are measured by Rosemount 2088G pressure transmitters with span accuracies of ±0.075%, or ±0.2 bar with a 276 bar span. Temperatures are measured by standard Type-K and Type-B thermocouples with accuracies of ± 0.5 K. Watlow electric resistance line heaters provide sufficient heat capacity to the CO_2 and O_2 streams to maintain a minimum preheat temperature of 330 K, but industrial process heater options have been identified to eventually increase preheat temperatures to 950 K.

The Allen-Bradley BPCS controls the process and provides process data acquisition with high reliability and availability, but at relatively low frequency (approximately 1 Hz). Collection of higher-frequency data (exceeding 4000 Hz) will be performed as needed using a separate National Instruments data acquisition system.

COMBUSTOR DESIGN

A simple combustor design was adopted based on previous designs of uni-element rocket combustors for research purposes [11, 12] and is shown in Figure 3. A single, fuel-centered coaxial injector was selected and sized to ensure fully turbulent flow and an oxidizer-to-fuel momentum flux ratio of 2.8 which is typical for gas-gas rocket injector elements. The fuel tube had an inside diameter of 2.08 mm with a lip size of 1.00 mm and the oxidizer gap was 1.67 mm (Figure 3b). The resultant fuel and oxidizer injection velocities are 11.4 and 21.4 m/s respectively for the baseline case of 100 kW and 80 bar with an oxidizer preheat temperature of 950K.

Simulations of both round and square combustion chambers showed only minimal differences in the flow field so a square chamber of 110 mm in length and 20 mm dimensions on each side was chosen as the best option to provide full optical access to the combustor for imaging and laser diagnostics. The walls of the combustor are effusion cooled with a porous copper liner with CO_2 flowing through with an inlet temperature of 300 K.

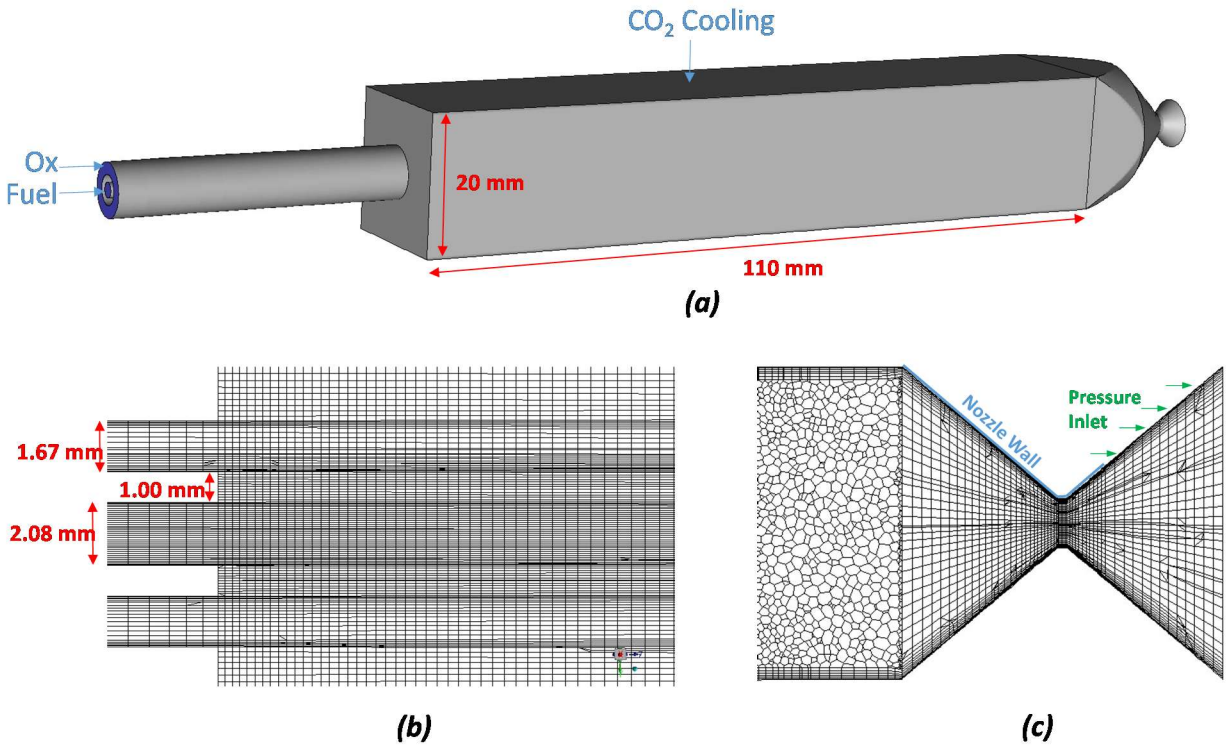

Figure 3: (a) Schematic of combustor, (b) injector mesh details and (c) nozzle mesh denoting walls and pressure entrainment inlet section.

A 10 mm long square to round transition section which is back side water cooled with a 3.175 mm copper wall is located at the end of the combustor section followed by a water cooled copper nozzle with a 3.17 mm diameter opening (Figure 3c). The nozzle dimensions were selected to generate a combustor pressure of 80 bar at the nominal 100 kW flow conditions. A short section downstream of the nozzle expansion is included as an entrainment inlet.

The 1.7M cell 3D computational domain consisted of a hex dominant mesh with polyhedral cells in the transition section. A boundary layer was included on the injector, combustor and nozzle walls with an initial cell size of 80 μm in order to resolve the boundary layer using conventional wall functions with the first layer placed at a y+ value of roughly 30. The nominal mesh size in the shear layer where mixing and reaction is occurring was selected based on initial Reynolds-Averaged Navier-Stokes (RANS) simulations to estimate the Taylor length scale which is at the lower end of the inertial range of turbulence and is typically used as a target resolution for Large Eddy Simulation (LES). The Taylor length scale is defined as; $\sqrt{10\nu\frac{k}{\varepsilon}}$, where ν is the kinematic viscosity, k is the turbulent kinetic energy and ε is the turbulent dissipation rate and was on the order of 120 μm.

COMPUTATIONAL APPROACH

ANSYS Fluent 22.1 [13] was used for the calculations presented here. An incompressible steady state RANS approach using a skeletal 16 species methane-oxygen mechanism was used along with a realizable k-ε turbulence model for most of the combustor simulations. The chemical kinetic mechanism was developed at the University of Central Florida [14] and is derived from the Saudi Aramco 2.0 detailed hydrocarbon mechanism developed by the National University of Ireland Galway [15] which has been validated against laminar flame speed data at pressure up to 60 bar [16] with methane, oxygen and helium and ignition delay time data up to 260 bar [17] with methane, oxygen and argon mixtures. The skeletal mechanism was shown to do reasonably well at predicting ignition delay time compared to the parent mechanism at conditions relevant to the Allam cycle [6].

No combustion sub-model was used which is equivalent to assuming that the sub-grid mixing is fast relative to the chemical reactions. Several simulations were run using a LES modeling approach as a means of examining turbulence effects using an implicit grid filter along with a transported kinetic energy equation sub-grid viscosity model.

For the combustor simulations, the nozzle section was not included and the combustor exit pressure was fixed at the desired value. A single, separate simulation using steady state compressible flow was run with the nozzle section included for the explicit purpose of investigating wall heat transfer and surface temperatures along with the prediction of combustor operating pressure.

For all the simulations, the SIMPLE pressure-velocity coupling method was used with second-order upwinding for the momentum and scalar equations. For the LES calculations the bounded central differencing method was used for the momentum equations and a bounded 2nd order implicit time marching scheme was employed. Fuel and oxidizer inlets were modeled as mass flow inlets and the combustor walls were modeled with the “perforated wall” model in Fluent with a uniform flow of CO_2

passing through the perforated layer with an inlet temperature of 300 K. The cooling flowrate was kept constant at 40.0 g/s for all of the cases studied here. For the incompressible simulations without the nozzle the combustor exit was modeled as a fixed pressure boundary. For the compressible simulation with the nozzle included the pressure was set at atmospheric downstream of the entrainment section.

Table 2: Operating conditions for the four cases studied.

	Case 1	Case 2	Case 3	Case 4
O_2 Mass Fraction in Oxidizer	0.3	0.3	0.3	0.3
Heat Input (kW)	100	100	25	25
Fuel Flow (g/s)	2.0	2.0	0.5	0.5
Oxidizer Flow (g/s)	26.68	26.68	6.67	6.67
U_{ox} (m/s)	21.4	7.4	5.3	1.9
Re_{ox}	34,700	85,200	8,670	21,300
U_{fuel} (m/s)	11.4	11.4	2.8	2.8
Re_{fuel}	64,600	64,600	16,100	16,100
T_{ox} (K)	950	330	950	330
Mom flux (ox/fuel)	2.82	0.98	2.82	0.98
CO_2 cooling (g/s)	40.0	40.0	40.0	40.0

Three basic operating conditions were selected which correspond to two power levels of 25 kW and 100 kW as well as two oxidizer preheat temperatures of 950 K and 330 K. The combustion facility is planned to be commissioned with a maximum oxidizer preheat temperature of 330 K with a planned heater upgrade that will allow for temperatures up to 950 K. Flowrates and bulk injection velocities are shown in Table 2.

The equivalence ratio was fixed at stoichiometric and the oxygen concentration in the injector was fixed at 30% by mass with the balance being CO_2. Also listed in the table are the fuel and oxidizer Reynolds numbers.

RESULTS AND DISCUSSION

Contours of temperature, CO mass fraction and heat release through the center of the combustor are shown in Figure 4 for Case 1, which is the baseline design case for the facility and combustor at the maximum design oxidizer preheat temperature of 950 K. The flame appears to be fairly long, extending into the combustor exit nozzle as evidenced by the open tip of the flame and heat release still occurring at the combustor exit. The combustion efficiency (CE) for this case as defined by the heat release normalized by the lower heating value of methane is 90.6 %. While there is virtually no methane exiting the combustor, there is a significant quantity of carbon monoxide with a mass-weighted exit mass fraction of 1.47%.

Figure 4(b) also presents results for the same case with the LES turbulence modeling approach. For the LES cases presented here, the simulations were time-averaged for several flow through times to derive mean quantities. These results seem to show a shorter flame length and more rapid mixing. The combustion efficiency was 94.4% for this case and the CO exit mass fraction was 1.7%.

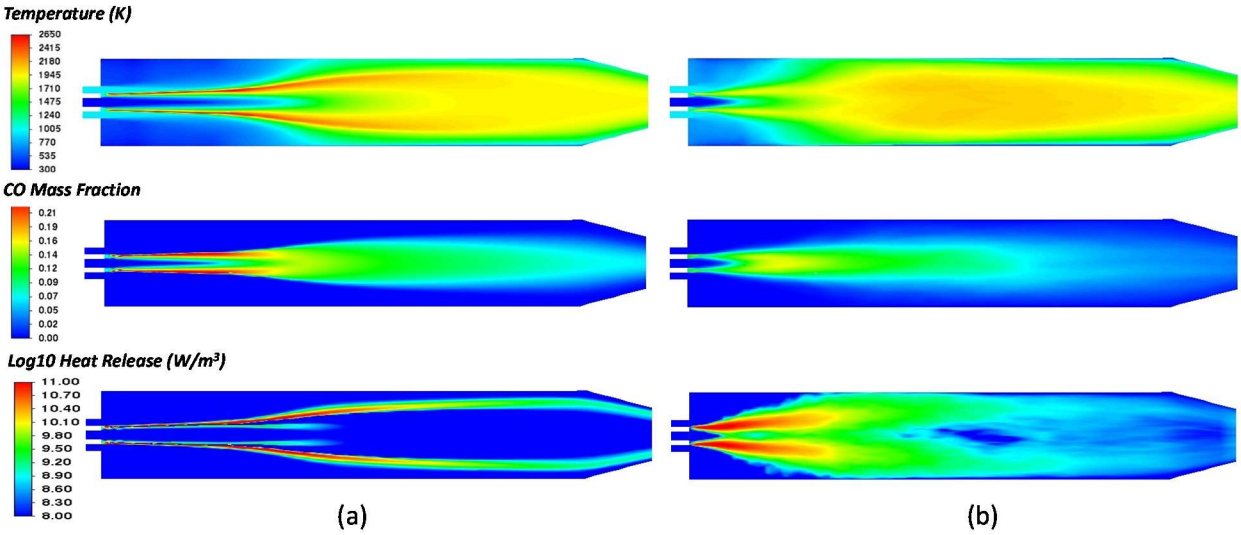

Figure 4: Contours of temperature (top), CO mass fraction (middle) and Log10 of the heat release (bottom) for: (a) RANS, and (b) LES model for Case 1 (100 kW, 950 K).

The next case presented is case 2, where the power input is maintained at 100 kW but the oxidizer preheat temperature is reduced to 330 K which is the target oxidizer temperature at facility commissioning. Figure 5(a) shows contour plots of temperature, CO mass fraction and heat release for this condition along with Case 1 (Fig. 5(b)). The combustion efficiency for this case was 64.5% and the CO exit mass fraction was 1.12%. For this case there was a significant flow of unburned methane exiting the combustor with a mass fraction of 0.81% representing 27.5% of the inflow of methane. While it is obvious that the combustor temperatures are significantly lower than Case 1 (Fig. 5(b)) which would result in slower chemical kinetics, the effect of the lower oxidizer preheat temperature on mixing are not clear.

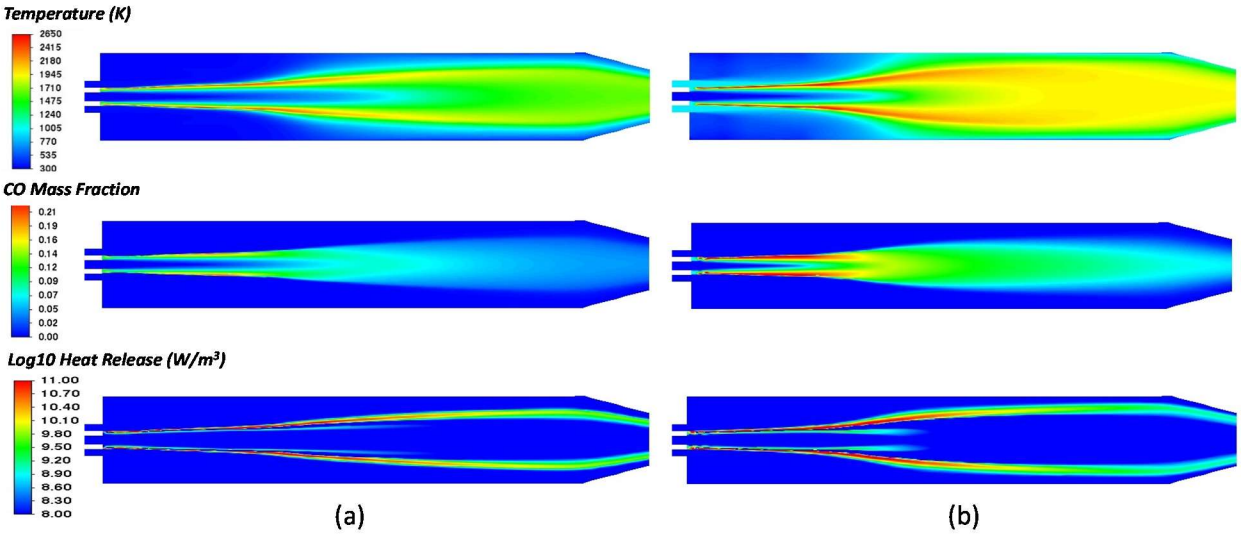

Figure 5: Contours of temperature (top), CO mass fraction (middle) and Log10 of the heat release (bottom) from the RANS simulations for: (a) Case 2 (100 kW, 330 K), and (b) Case 1 (100 kW, 950 K).

To better understand this effect, two non-reacting simulations were run for the conditions of Cases 1 and 2. The mixing was characterized by the area-weighted average uniformity index of CH_4 at various distances from the injector tip. The uniformity index is defined as;

$$UI_{CH4} = 1 - \frac{\sum[|Y_{CH4} - \overline{Y_{CH4}}|A]}{2|\overline{Y_{CH4}}|\sum A} \quad (1)$$

where a value of 1 would represent perfect mixing. From this definition, a "mixing length" was defined as the distance from the injection point to the plane where the uniformity index (UI_{CH4}) reached a value of 0.8. For Case 1, with a preheat temperature of 950 K, this was 34 mm. For Case 2, with a preheat of 330 K, the mixing length was 53 mm. The faster mixing for the higher preheat temperature is believed to be due to the higher oxidizer injection velocity and nearly three-fold higher momentum flux ratio.

The effect of fuel flowrate is shown in Figure 6 which shows a comparison of Case 1 with a fuel input of 100 kW and case 3 with a fuel input of 25 kW, both with an oxidizer preheat temperature of 950 K using the RANS approach. As the fuel input was lowered from 100 kW to 25 kW the combustion efficiency dropped from 90.6% to 66.3% with about 15% of the fuel exiting the combustor unburned for the lower fuel flow case. While some of this decrease in combustion efficiency can be explained by the lower injection velocities for Case 3, some of this effect could be due to the lower combustor exit temperature which dropped from 1498 K to 664 K as a result of the constant wall cooling CO_2 flowrate of 40 g/s. The lower temperature has an effect not only on the chemical kinetics but also the bulk velocity and thus mixing in the combustor.

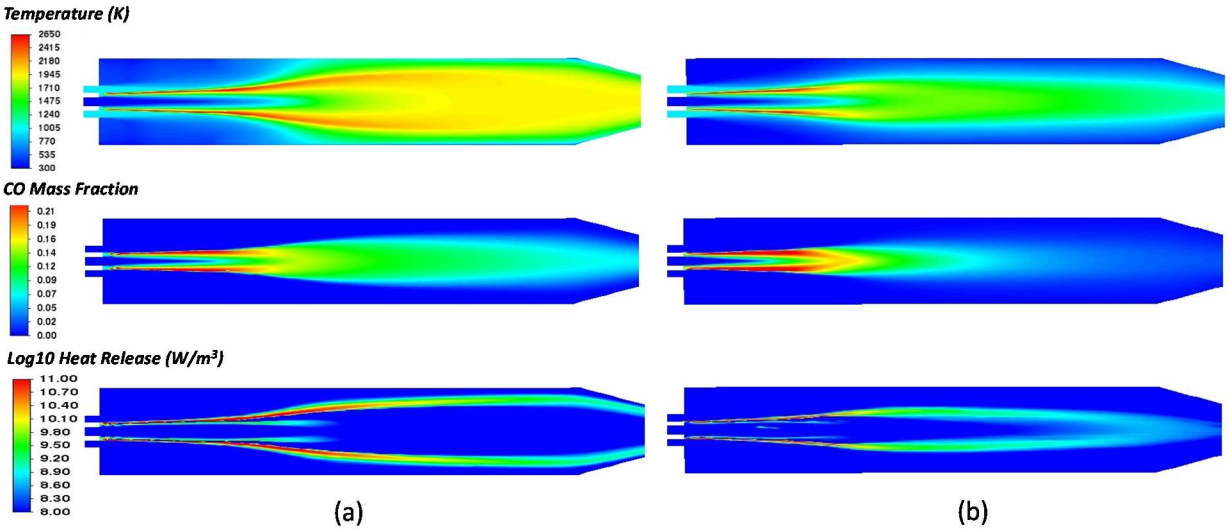

Figure 6: Contours of temperature (top), CO mass fraction (middle) and Log10 of the heat release (bottom) from the RANS simulations for: (a) Case 1 (100 kW, 950 K), and (b) Case 3 (25 kW, 950 K).

Case 4 is for the 330 K oxidizer preheat temperature but at ¼ of the power input of Case 2. Figure 7 contains contour plots of temperature, CO mass fraction and heat release for both the RANS and LES turbulence modeling approaches. It is clear from this comparison that RANS approach predicts a much longer flame length compared to the LES approach. It appears that the realizable k-ε model may over-predict the dissipation of turbulent kinetic energy resulting in poorer mixing and a much longer mixing length. This result clearly shows the need for model validation at these conditions.

The next study was on the effect of operating pressure on the flame characteristics. Variations of Case 4 were run with three different combustor operating pressures of; 80, 60 and 40 bar by scaling all of the flow rates down from the 80 bar condition to maintain the same injection velocity at each pressure. For instance, the 40 bar case had half the flowrate of the 80 bar case. Figure 8 shows a comparison of the heat release profiles for the three cases and it is clear that pressure has a fairly minor effect on the heat release distribution through the increased reaction rates at the higher pressures. For these three cases the combustion efficiency only increased from 41.1 % to 43.7 % as pressure was increased from 40 to 80 bar. The mass fraction of CO was roughly 0.62 % for all three cases.

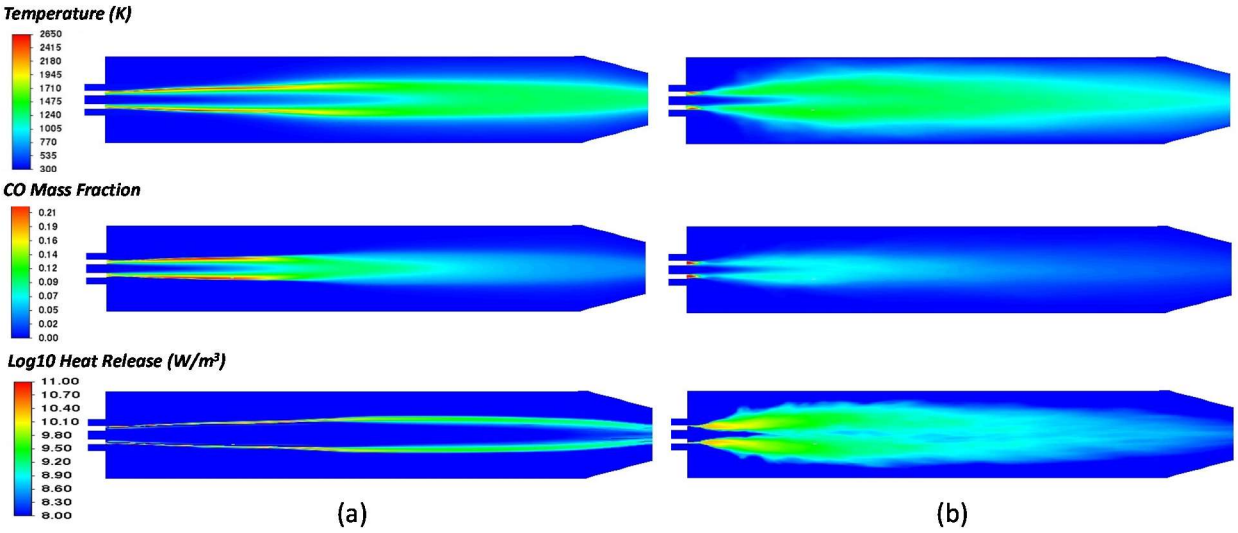

Figure 7: Contours of temperature (top), CO mass fraction (middle) and Log10 of the heat release (bottom) for: (a) RANS, and (b) LES model for Case 4 (25 kW, 330 K).

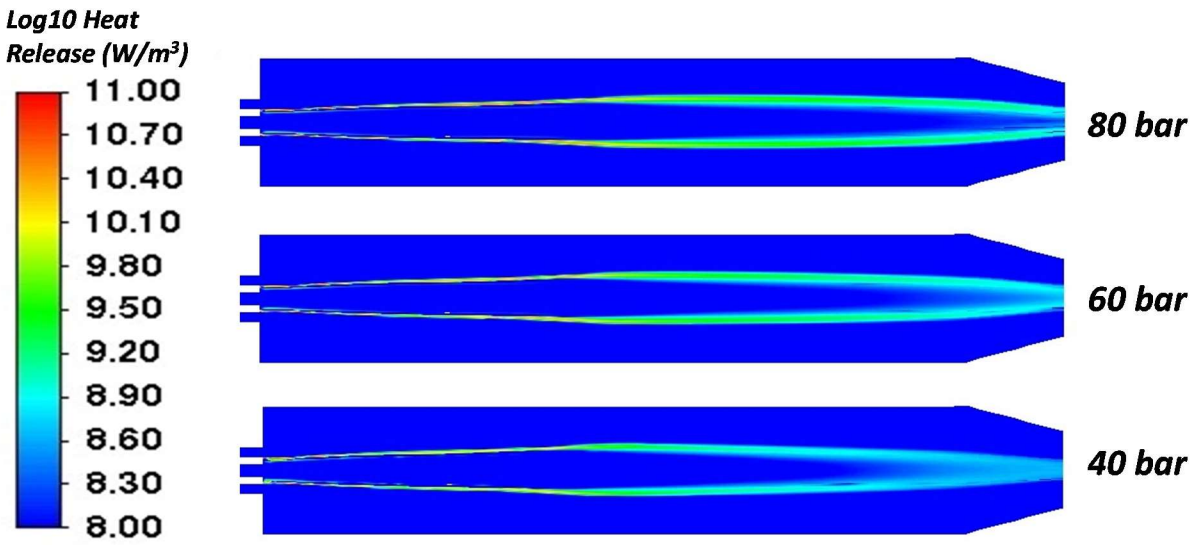

Figure 8: Contours of Log10 of the heat release from the RANS approach for 330K oxidizer preheat temperature and: 25 kW/80 bar (top), 18.8 kW/60 bar (middle), and 12.5 kW/40 bar (bottom).

The last study conducted was on an alternative injector design. As the simple shear-coaxial injector design is expected to provide good validation data for flame anchoring, liftoff, and flame length, it is not an ideal design for promoting good mixing and combustion efficiency. A simple modification was made that required no changes to the modeled geometry by swirling the oxidizer at the inlet boundary. A swirl angle of 45° was adopted meaning that the axial and tangential velocity components were equal. The resulting flow field includes recirculation zones within the combustor and much faster mixing. Results for Case 1 with both the RANS and LES modeling approach are shown in Figure 9 and show a much shorter flame length with the bulk of the heat release occurring on the first 30 mm of the combustor. For the RANS simulation, the combustion efficiency was 98.2% which was significantly higher than the non-swirl case (90.6 %) and the CO exit mass fraction was 0.26% which is much less than the non-swirl cases (1.47%). This can be directly attributed to the much improved mixing and subsequent burnout of CO into CO_2. For the LES case shown in Fig. 9 the combustion efficiency was 98.7% and the CO exit mass fraction was 1.4%

Also note in Figure 9 that there is much more similarity between the RANS and LES results compared to the shear-coaxial results shown in Fig. 4. This could be the result of the much improved mixing of the swirl design being less sensitive to turbulence modeling approach.

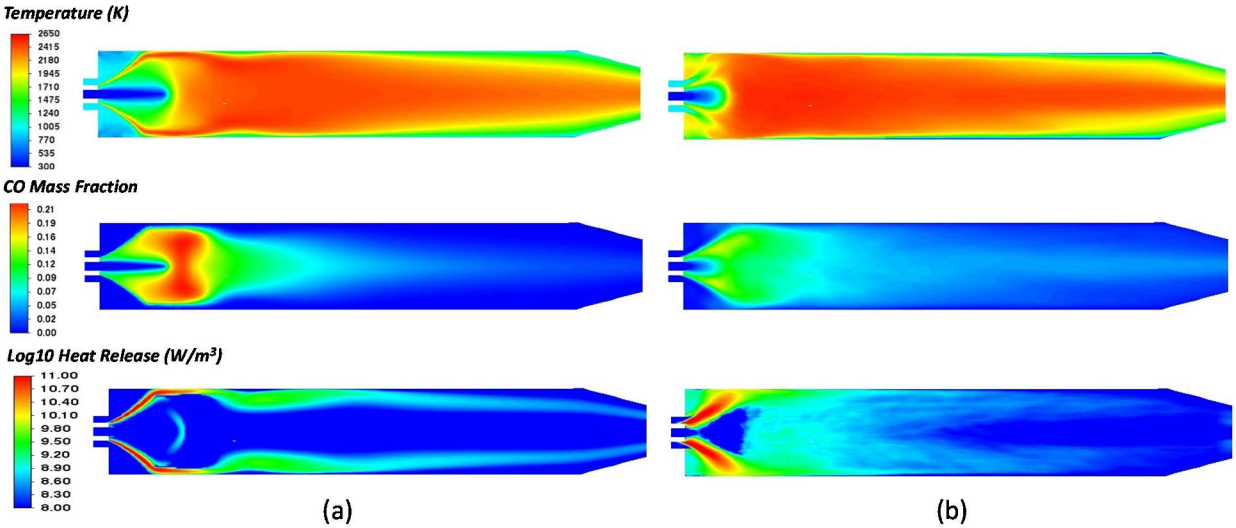

Figure 9: Contours of temperature (top), CO mass fraction (middle) and Log10 of the heat release (bottom) for: (a) RANS, and (b) LES model for Case 1 (100 kW, 950 K).

Simulations with the swirl injector approach were also run for Case 4 which showed the poorest combustion efficiency with the non-swirling oxidizer injection (Fig. 7). Results for this case are shown in Figure 10. For both the RANS and LES results shown in Fig. 10, the combustion efficiency was around 63% which is a modest improvement over the non-swirl case (CE=43%). Much of this can be attributed to unburned CH_4 exiting the combustor which was 27% of the inlet CH_4 flow for the RANS case and 32% for the LES case shown in Fig. 10. The remaining inefficiency is attributed to incomplete combustion with the product being CO rather than CO_2. For both cases roughly 28% of the CH_4 flowing into the combustor was converted to CO with the remaining being unburned or converted to CO_2.

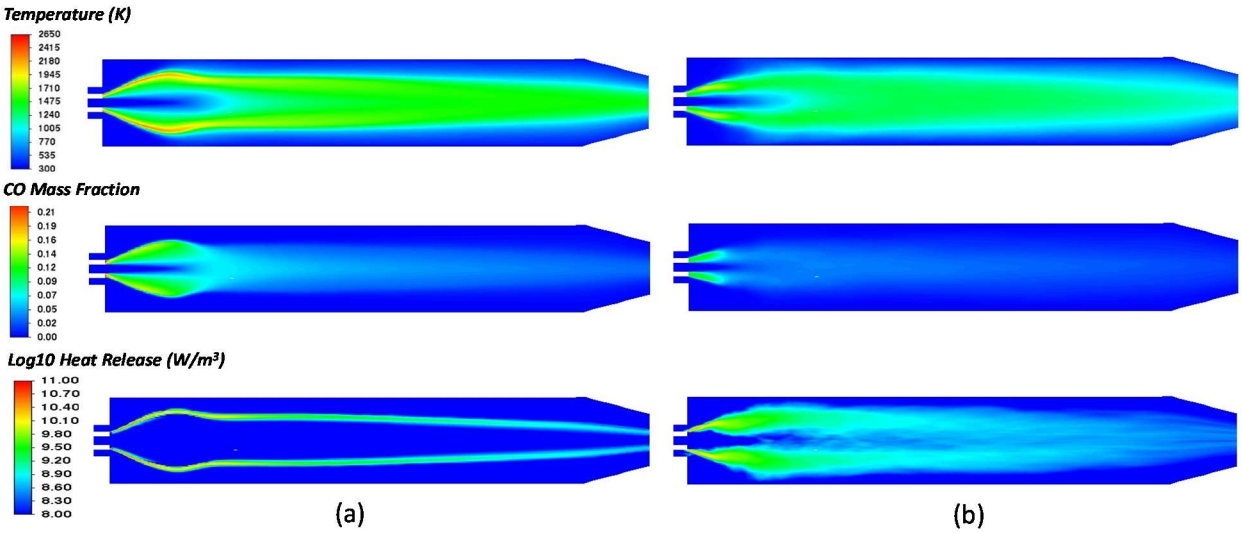

Figure 10: Contours of temperature (top), CO mass fraction (middle) and Log10 of the heat release (bottom) for: (a) RANS, and (b) LES model for Case 4 (25 kW, 330 K).

Finally, results for the combustor simulation with the exit nozzle attached using the compressible flow formulation are presented in Figure 11 for the conditions of Case 1. The nozzle throat diameter of 3.17mm was able to generate a combustor pressure of 77.3 bar, which was close to the target pressure of 80 bar. The transition section and nozzle wall are backside water cooled through a copper combustor wall of 3.175 mm thickness while the combustor walls are effusion cooled through the use of a porous copper liner with CO_2 flowing through it at an inlet temperature of 300 K. The simulation shows that this cooling approach does an excellent job of maintaining the wall temperatures at an acceptable value with the peak temperature of 460 K occurring at the nozzle throat which well below the maximum usage temperature for copper which is typically cited as 530 K.

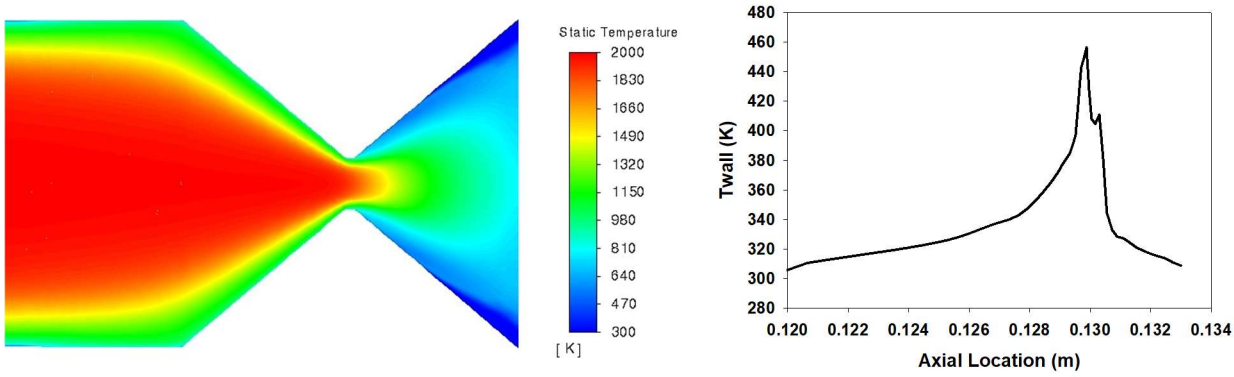

Figure 11: Contours of static temperature (a) for compressible RANS simulation for Case 1 with the nozzle attached. Plot of peak wall temperature (b) vs. axial location through the nozzle.

SUMMARY AND CONCLUSIONS

An experimental facility currently under construction at NETL to study high-pressure (80 bar) oxy-combustion and to provide model validation data has been described along with details of the combustor test article. CFD simulations of the target combustor geometry have also been presented including key combustor performance metrics including combustion efficiency and carbon monoxide emissions. The data generated in this facility is intended to be a model validation "stepping-stone" to higher pressures more representative of Allam cycle conditions (300 bar).

The CFD simulations show that significant variations in combustion efficiency can be attributed to differences is mixing as combustor output power and oxidizer preheat temperature are varied. Further variations through swirling of the oxidizer flow showed a dramatic improvement in mixing and combustion efficiency and a subsequent reduction in CO emissions. Results for all of the cases studied here are presented in the appendix.

The facility is currently under construction and is planned to be completed by the end of 2022. Combustor fabrication is planned to begin as well in late 2022 and testing to commence in late 2023.

APPENDIX

Table 3: Summary of all simulation results. LES results are time-averaged. Exit quantities are mass-weighted averages. Heat loss is to walls of combustor and nozzle.

Case	Swirl?	kW	P(bar)	T ox(K)	Turb	Fuel Flow (g/s)	Heat Release (W)	Comb Eff (%)	Heat Loss (W)	T exit (K)	Y co
Case 1	No-Swirl	100	80	950	RANS	2	90570	90.57	5383	1498	0.0147
Case 1	No-Swirl	100	80	950	LES	2	94360	94.36	2590	1581	0.0172
Case 2	No-Swirl	100	80	330	RANS	2	64480	64.48	821	1053	0.0112
Case 2	No-Swirl	100	80	330	LES	2	69355	69.36	603	1207	0.0121
Case 3	No-Swirl	25	80	950	RANS	0.5	16569	66.28	199	664	0.0072
Case 4	No-Swirl	25	80	330	RANS	0.5	10925	43.7	87	519	0.0063
Case 4	No-Swirl	25	80	330	LES	0.5	15115	60.46	120	632	0.0064
Case 1	Swirl	100	80	950	RANS	2	98209	98.21	1510	1613	0.0026
Case 1	Swirl	100	80	950	LES	2	98740	98.74	1310	1632	0.0140
Case 4	Swirl	25	80	330	RANS	0.5	15824	63.30	78	613	0.0054
Case 4	Swirl	25	80	330	LES	0.5	15681	62.72	121	612	0.0054
Case 3	Swirl	25	80	950	RANS	0.5	22704	90.82	563	818	0.0044
Case 3	Swirl	25	80	950	LES	0.5	23703	94.81	182	861	0.0046
Case 4 (scaled)	No-Swirl	18.8	60	330	RANS	0.375	7986	42.592	68	517	0.0063
Case 4 (scaled)	No-Swirl	12.5	40	330	RANS	0.25	5140	41.12	48	513	0.0061

ACKNOWLEDGEMENTS

This work was supported by the NETL Turbines Field Work Proposal awarded by the US DOE Office of Fossil Energy and Carbon Management (FECM). The authors would like to acknowledge the DOE Advanced Turbines Program Technology Manager Mr. Richard Dennis.

DISCLAIMER

This work was funded by the Department of Energy, National Energy Technology Laboratory, an agency of the United States Government. Neither the United States Government nor any agency thereof, nor any of their employees makes any warranty, expressed or implied, or assumes any legal liability or responsibility for the accuracy, completeness, or usefulness of any information, apparatus, product, or process disclosed, or represents that its use would not infringe privately owned rights. Reference herein to any specific commercial product, process, or service by trade name, trademark, manufacturer, or otherwise, does not necessarily constitute or imply its endorsement, recommendation, or favoring by the United States Government or any agency thereof. The views and opinions of authors expressed herein do not necessarily state or reflect those of the United States Government or any agency thereof.

REFERENCES

1. S. Patel, “Breakthrough: NET Power’s Allam Cycle Test Facility Delivers First Power to ERCOT Grid”, Power Magazine, Nov. 18, 2021.

2. P.A. Strakey, “Oxy-Combustion Modeling for Direct-Fired sCO_2 Power Cycles” *Journal of Energy Resources Technology*, Vol. 141, July, 2019.
3. P.A. Strakey, “Oxy-Combustion Flame Fundamentals for Supercritical CO2 Power Cycles”, Presented at the 6th International Supercritical CO2 Power Cycles Symposium, March 27-29, 2018, Pittsburgh, PA.
4. Oleg A. Evdokimov “A development and Numerical Study of a High-Pressure Gas Turbine Combustion Chamber Based on Mesoscale Coaxial Swirling Jets”, *Int. J. Energy Clean Environ.*, Vol 23, no. 3, 2022, pp. 55-76. **DOI:** 10.1615/InterJEnerCleanEnv.2022041397.
5. Yeshayahou Levy and P. Arfim “Turbuence-Chemistry Interaction Calculations for Improved NOx Predictions”, *Int. J. Energy Clean Environ.*, Vol 6, no. 3, 2005, pp. 195-224. **DOI:** 10.1615/InterJEnerCleanEnv.v6.i3.10.
6. Allam, R. J., *et. al*., “High Efficiency and Low Cost of Electricity Generation From Fossil Fuels While Eliminating Atmospheric Emissions, Including Carbon Dioxide”, *Energy Procedia*, **37,** 2013, pp. 1135-1149.
7. Allam, R.J., Fetvedt, J.E., Forrest, B.A. and Freed, D.A., “The Oxy-Fuel, Supercritical CO2 Allam Cycle: New Cycle Developments to Produce Even Lower-Cost Electricity from Fossil Fuels Without Atmospheric Emissions”, Proceedings of ASME Turbo Expo 2014, GT2014-26952, June 16-20, Dusseldorf, Germany.
8. J. Barrie, K.Brown, P.R. Hatcher and H.U. Schellhase, “Carbon Dioxide Pipelines: A Preliminary Review of Design and Risk”, Greenhouse Gas Control Technologies 7, Proceedings of the 7th International Conference on Greenhouse Gas Control Technologies, 5-September 2004, Vancouver, Canada, Volume I, 2005, Pages 315-320.
9. Jacob Delimont, Aaron McClung and Marc Portnoff, “Direct Fired Oxy-Fuel Combustor for sCO_2 Power Cycles: 1MW Scale Design and Preliminary Bench Top Testing*”, ASME Turbo Expo: Power for Land, Sea, and Air*, GT2017-64952, June 26-30, 2017, Charlotte, NC. DOI: 10.1115/GT2017-64952.
10. P.J. Linstrom and W.G. Mallard, Eds., **NIST Chemistry WebBook, NIST Standard Reference Database Number 69**, National Institute of Standards and Technology, Gaithersburg MD, 20899, https://doi.org/10.18434/T4D303, (retrieved June 14, 2022).
11. A. Dasari, L. W. White, Y. M. Abul-Huda and M. Gambo, “Experimental Characterization of the Flowfield and Flame Structure in a Rocket Combustor Using OH-PLIF”, Proceedings of the Combustion Institute-Canadian Section, Spring Technical Meeting, Univ. Windsor, May 12-15,2014.
12. R.K. Cohn, P.A. Strakey, R.W. Bates, D.G. Talley, J.A. Muss and C.W. Johnson, "Swirl Coaxial Injector Development", Presented at the *41st AIAA Aerospace Sciences Meeting and Exhibit*, Reno, NV, January 2003.
13. ANSYS Fluent, Release 22.1.
14. K.R.V. Manikantachari, V. Ladislav, S. Martin, J.O. Bobren-Diaz and S. Vasu, “Reduced Chemical Kinetic Mechanisms for Oxy/Methane Supercritical CO2 Combustor Simulations”, *J. Energy Resources Technology*, Vol. 140, Is. 9, 2018.
15. W.K. Metcalfe, S.M. Burke, S.S. Ahmed, H.J. Curran, " A hierarchical and comparative kinetic modeling study of C1–C2 hydrocarbon and oxygenated fuels”, *Int. J. Chem. Kinet.* (2013) 45(10) 638–675.
16. G. Rozenchan, D.I. Zhu, C.K. Law and S.D. Tse “Outward Propagation, Burning Velocities, and Chemical Effects of Methane Flames up to 60 atm”, *Proc. Comb. Inst.*, Vol. 29, 2002, pp. 1461-1469.
17. E.L. Petersen, D.F. Davidson and R.K. Hanson, “Ignition Delay Times of Ram Accelerator CH4/O2/diluent Mixtures”, *J. Prop. Power*, Vol. 15, No. 1, pp.82-91, 1999.